electronics

MDPI

Article

High-Speed Non-Volatile Optical Memory: Achievements and Challenges

Vadym Zayets

Spintronics Research Center, National Institute of Advanced Industrial Science and Technology (AIST), Tsukuba 305-8568, Japan; v.zayets@aist.go.jp; Tel.: +81-298-615-426

Academic Editor: Matteo Cantoni
Received: 31 October 2016; Accepted: 28 December 2016; Published: 10 January 2017

Abstract: We have proposed, fabricated, and studied a new design of a high-speed optical non-volatile memory. The recoding mechanism of the proposed memory utilizes a magnetization reversal of a nanomagnet by a spin-polarized photocurrent. It was shown experimentally that the operational speed of this memory may be extremely fast above 1 TBit/s. The challenges to realize both a high-speed recording and a high-speed reading are discussed. The memory is compact, integratable, and compatible with present semiconductor technology. If realized, it will advance data processing and computing technology towards a faster operation speed.

Keywords: high-speed optical memory; spin-transfer torque; ferromagnetic-metal/semiconductor hybrid; nanomagnet; spin-polarized current; high-speed electron transport

1. Introduction

Data processing and transmission needs ever-faster operational speed. The transfer rate of 25.4 TBit/s through a single optical fiber was demonstrated [1]. However, due to the speed limitation of present electronic components, the data is transferred using many channels at different optical frequencies. Since each channel needs individual electrical and electro-optical components, such a system is complex, expensive, and has high power consumption. With the availability of ultra-fast optical non-volatile memory, the high broadband of optical fibers can be used in a wider range of applications, and a significant reduction in power consumption for data processing could be expected. High-speed data processing, chip-to-chip optical connections, and optical buffer memory are a few of the possible applications of a high-speed non-volatile optical memory.

A high-speed non-volatile optical memory is an essential component to achieve the required high-speed data processing. There are two major applications of this memory.

The first important application of the high-speed memory is chip-to-chip interconnection [2,3]. Its purpose is to transfer data from one silicon chip to another in the shortest possible time. In a silicon chip electrical memory, like Dynamic random-access memory (DRAM), Static random-access memory (SRAM), Phase-change memory (PRAM), Flash, Resistive random-access memory (ReRAM) [4] and Magnetoresistive random-access memory (MRAM) [5] , is dense, but electrical memory has a relatively moderate operational speed. The moderate speed for the data transfer inside the chip is acceptable and it does not limit a high speed of the total data transfer inside a chip. This is because, inside the chip, there is a large number of connection lines and the data transfer happens in parallel. Even though the transfer speed of each line is moderate, the overall transfer speed is fast. The case of a chip-to-chip interconnection is different, because the number of connection lines between chips is limited. It is important to transfer data through each line at a substantially faster speed. Optical interconnections between chips are used [2,3] in order to achieve a high-speed data transfer. A high-speed optical buffer memory is required to efficiently utilize the high-speed capabilities of the optical data links.

The purpose the buffer memory is to match the in-parallel data transfer inside a chip with the in-serial data transfer between chips. The buffer memory does not need to be dense, but it must be very fast.

Another important application of the proposed high-speed optical memory is a buffer memory for an optical network router. It is worth noting that even though high-speed optical fiber links are widely installed worldwide, only a small fraction of their high-speed capacity is used. At present, the speed of a network is mostly limited by the speed of the network routers. The network router switches data streams between different nodes in a network. The function of the network router is to receive the data package from one channel, to store it, and send it to the second channel. Since the availability of the second channel is basically unknown, non-volatile memory has to be used in the router. Routers made of electrical components are installed in modern optical networks. Routers, which can process data at speeds up to 10 GBit/s, are already commercially available. Now significant efforts are applied to fabricate routers that can process data at speeds of 40 GBit/s. It is a challenging task, because the required operational speed is significantly above the speed limit of most of the electrical components. A further possible increase of the operational speed of the router, which is made of electrical components is, therefore, questionable. The use of a high-speed non-volatile optical memory might be the only option to increase the operational speed of an optical router and subsequently to increase the overall speed of the Internet [6].

It should be noted that the operation functions of a high-speed optical memory are different from the operation functions of a conventional random-access memory. In the random-access memory the reading and writing of one data bit can be done in any memory cell once per clock cycle. In contrast, in a high-speed optical memory a package of data pulses is read or recorded per clock cycle. The data pulses in a package should be as short as possible with a shortest-possible interval between them. Pulses with widths and intervals of a few picoseconds or shorter should be used. The interval between events of reading and writing a package is longer. It is about a few nanoseconds long. According to these operational features, the recording process in a high-speed optical memory is divided into two steps of substantially different operational speeds (Figure 1). The first step is called demultiplexing. During this step a package of data pulses is redistributed into individual memory cells ensuring that only one pulse is memorized per each memory cell. Since the data pulses in the package are very close to each other, the fastest-possible operational speed is required for demultiplexing. As it is shown below, the unique high-speed properties of the spin allows the successful demultiplexing for pulses with period as short as 450 ns. This corresponds to the operational speed of 2.5 TBit/s. The second recording step is memorizing each data pulse into each individual memory cell. This step can take a longer time. The time of the second step is only limited by the interval between data packages, which is relatively long. In the proposed memory, the duration of the second step is the magnetization reversal time of a nanomagnet. It is about 1 ns.

It should be noted that a high-speed non-volatile optical memory is not commercially available. Even the full memory performance, including high-speed reading, demultiplexing, and writing, has not been yet demonstrated in a single device. At present, a switchable delay line is used as an optical buffer memory [6–8]. A very short storage time of about a few milliseconds is a significant limitation of this memory. Another interesting design of a high-speed optical memory is optical RAM [9,10]. It combines a high-speed demultiplexer with a conventional electrical SRAM memory [9] or an optical-cavity memory [10]. The operation principle of the used high-speed demultiplexer is based on the saturable absorption in low-temperature-grown (LT-) InGaAs/AlGaAs quantum wells. The large size of this memory and the lack of integration make the possibility of commercialization of this memory questionable. The maximum operational speed of a demultiplexer based on the saturable absorption in LT-III-V's is limited by the absorption recovery time, which is about 20–100 ps. This time corresponds to the switching speed of 10–50 GBit/s. By optimizing the absorber structure and utilizing a spin-selective pumping, the demultiplexer speed of 1000 GBit/s has been demonstrated [11]. However, such operation beyond physical limits might not be reliable and the slower operational speed of 40 GBit/s [9,10] was only reported for the memories, which utilize a saturable absorber.

The operational speed of the demultiplexer of the memory, which is described in this paper, is experimentally verified to be 2200 GBit/s. The recording speed of this memory is only limited by the electron dephasing time, which is at least shorter than 450 fs [12].

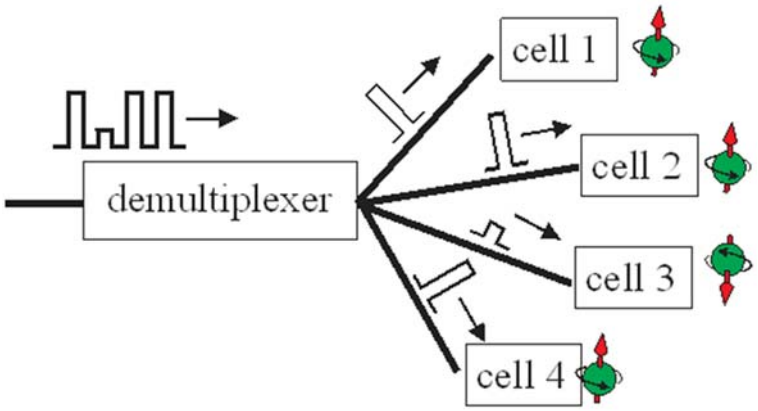

Figure 1. Recording mechanism of a high-speed memory, which consists of two steps. High-speed Step 1: Demultiplexer separates each data pulse in the package into an individual memory cell; Moderate-speed Step 2: Each-pulse is stored in each cell for long-time storage.

This paper does not describe the performance of all memory functions measured in a single memory device. Instead it describes the requirements, achievements, challenges, and features of fabrication technology for each particular function of the proposed high-speed non-volatile optical memory. Each memory function has been studied in separately-fabricated devices.

In this paper two designs of the memory are described. In the first design an iron nanomagnet is used as a storage element. In the second design a magnetic tunnel junction (MTJ) is used as storage. Both designs are very similar. However, each design has its own advantages and disadvantages. The full performance of the proposed memory, including the demultiplexing, high-speed reading, high-speed spin injection and magnetization reversal, has not been demonstrated in a single device. Some functions were demonstrated in the design with a nanomagnet, some functions were demonstrated in the design with a MTJ and some functions still have to be demonstrated. The fabrication technologies of the memory with a nanomagnet and a MTJ have their own features and challenges. Therefore, each fabrication technology is described separately.

2. Memory Design, Fabrication, and Recording Principle

The memory consists of micro-sized memory cells integrated on a semiconductor wafer. A bit of data is stored by each cell. Each cell consists of three parts: an optical waveguide, a semiconductor-made photo detector, and a nanomagnet made of a ferromagnetic metal. In the case of the memory with MTJ, instead of a single layer of ferromagnetic metal two layers are used, which are separated by a tunnel barrier. Figure 2 shows a memory cell of a prototype fabricated on GaAs substrate. The AlGaAs waveguide is transparent for light of λ = 800 nm. It is used to deliver the optical pulses to the memory cell. On top of the AlGaAs waveguide the p-i-n GaAs photo-detector is fabricated. The photo-detector absorbs the light. On the top of GaAs photo detector there is a Fe nanomagnet. The size of the nanomagnet is sufficiently small so that it is a single-domain state and it has two stable magnetization directions along its easy axis. The data is stored as a magnetized direction in the nanomagnet. Additionally, the nanomagnet functions as a top contact for the photo-detector.

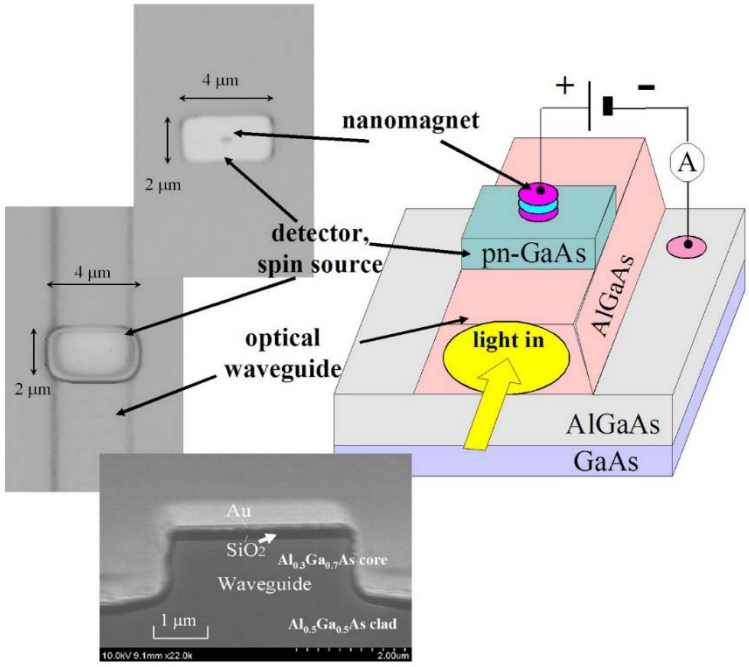

Figure 2. Memory cell of a prototype fabricated on GaAs substrate. The transparent AlGaAs waveguide is used to deliver optical pulses to the memory cell. The p-i-n GaAs photodetector absorbs the optical pulses. It converts spin information in an optical pulse into the spin polarization of photo-excited electrons. The data is stored as a magnetized direction in the nanomagnet, which is fabricated on top of the detector. The nanomagnet is also used as a top electrode for the detector.

The waveguide and the photo-detector were grown by a molecular-beam epitaxy (MBE) on a p-GaAs substrate. Following atomic-hydrogen cleaning and oxide removal, a 3-μm $Al_{0.5}Ga_{0.5}As$ cladding layer and a 3-μm $Al_{0.5}Ga_{0.5}As$ waveguide core layer were grown at T_{sub} = 650 °C. Both the core and cladding layers of the waveguide were slightly p-doped to about 7×10^{16} cm^{-3}. The p-i-n GaAs photo detector was grown at T_{sub} = 580 °C and a gradual doping was used. The doping is $p = 7 \times 10^{16}$ cm^{-3} at the interface of waveguide and it is gradually reduced to 2×10^{15} cm^{-3} over 200 nm. Next, a 500 nm of undoped GaAs was grown following by a 300 nm of n-GaAs ($n = 3 \times 10^{17}$ cm^{-3}). On the top of the detector a delta-doped contact layer was grown. The purpose of the contact layer is to create the lowest contact resistance between the detector and the nanomagnet. The contact layer consists of 25 nm of nn-GaAs (3×10^{19} cm^{-3}) and 12 nm nn-$In_{0.4}Ga_{0.6}As$ (7×10^{19} cm^{-3}). The InGaAs was grown at T_{sub} = 540 °C. The growth was 2D type. The InGaAs thickness, In-concentration and doping concentration were optimized so that a slight increase of either of parameters causes a growth change from a 2D- to a 3D-type.

After the growth of the photo-detector, the sample was transferred into a sputtering chamber without the breaking of vacuum. A 2 nm of Fe and a 4 nm of Au protection layer were deposited at $T_{sub} = -10$ °C. The nanomagnet with an ellipse-shape of 100 nm × 80 nm was fabricated using EB lithography and an Ar milling. The Fe nanomagnet was etched precisely up to the semiconductor interface. A 65-nm SiO_2 isolation layer aside of the nanomagnet was fabricated by the lift-off technique. Next, a 4 μm × 4 μm detector was wet-etched and a 4-μm-wide 1.8-μm deep waveguide was dry-etched. The Ti/Pt/Au p-type Ohmic contact was fabricated on the backside of the substrate. The sample was cleaved into 3-mm-long pieces across the waveguides. A reverse bias voltage for the photo detector was applied between the nanomagnet and the back contact. Light from a tunable Ti: sapphire laser was coupled into a fiber and from the fiber into the waveguide. Both the TE- and TM-polarized modes were excited with about the same amplitude. The fiber paths of TE- and TM-polarized light were separated. A phase modulator was installed in the fiber path of TM-polarized light. It was used to

adjust mutual phase between TM and TE modes in waveguide to make circular-polarized light at a point where it is absorbed by the detector.

For the data recording, the magnetization direction must be reversed by optical pulse. The circularly-polarized optical pulse is absorbed in the semiconductor detector creating spin-polarized electrons. Under applied voltage these spin-polarized electrons are injected from the detector into the nanomagnet. The spin transfer torque is a consequence of the transfer of spin angular momentum from a spin-polarized current to the magnetic moment of a nanomagnet. If the torque is sufficient, the magnetization turns and the data is memorized. Due to the optical selection rule, the spin-polarized electrons can be created only by the circular polarized optical pulse. The linear polarized light excites equal amounts of electrons of both up and down spins; therefore, there is no net spin polarization, the current injected into nanomagnet is not spin-polarized, and there is no spin torque.

Figure 3 shows integration of two memory cells and explains principle of high speed recording. There are two waveguide inputs. One input is for data pulses and one input is for the clock pulse. The clock pulse is used to select for recording a single pulse from a sequence of the data pulses. Polarization of data pulses and the clock pulse are linear and mutually orthogonal. Optical paths were split so each memory cell is illuminated by the data pulses and the clock pulse. The lengths of waveguides are adjusted so that the phase difference between the clock and data pulses is lambda/4 at each memory cell. At the first memory cell the clock pulse came at the same time with first data pulse. Therefore, these two pulses are combined into one circularly polarized pulse. Since only the first pulse is circularly polarized, only this pulse excites spin-polarized electrons, changes magnetization, and is memorized. All other data pulses are linearly polarized, they do not excite spin-polarized electrons and they have no effect on the magnetization. For the second memory cell, the clock pulse is slightly delayed relative to the data pulses and it comes together with the second data pulse. Only the second pulse is circularly polarized and can be memorized by the second memory cell. Therefore, each data pulse can be memorized by individual memory cell. The closer the pulses can be placed relative to each other, the more data can be transformed through one line and the faster recording speed of the memory can be achieved. The minimum interval between pulses, at which a pulse can be recorded without any influence of nearest pulse, determines the recording speed of the memory.

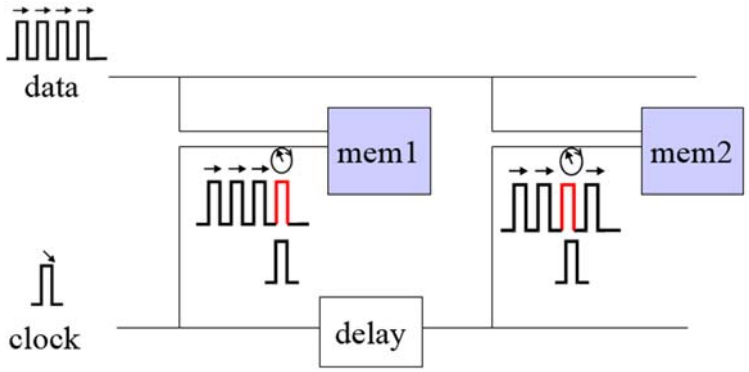

Figure 3. Integration of two memory cells and the principal of high-speed recording. Reproduced with permission from [12], American Institute of Physics, 2009.

It is impossible to make a demultiplexer with an infinite operational speed. A relaxation time of a switching mechanism always limits the operational speed. A switching mechanism of the shortest relaxation time should be used for the demultiplexing. The relaxation time for the switching of spin-polarization, which is the demultiplexing method in the proposed memory, is very short. As is shown below, it is about a few hundred femtoseconds. It is a unique property of the spin. The ultra-short relaxation time for the spin switching makes this switching mechanism well-suitable for use in ultra-high-speed optical devices.

The fast demultiplexing speed of the proposed memory was experimentally verified [12]. A package of two 100-fs-wide pulses with a period of 450 fs was combined with a 100-fs-wide clock pulse and was focused into a GaAs film. The spin polarization of the photo-excited electrons was measured by the Kerr rotation of a probe pulse. The clock pulse and pulses of the package were linearly cross-polarized. A delay between clock pulse and the package was controlled. Figure 4 shows the measured spin polarization of the photo-excited electrons as the function of the delay of the clock pulse in respect to the first pulse of the package. When the clock pulse was delayed so that it coincides with the first pulse of the package, the first pulse becomes a circularly-polarized. Only this pulse excites the spin-polarized photo-electrons and only this pulse is detected. The second pulse remains the linearly-polarized and it does not affect the recording. When the clock pulse is delayed to coincide with the second pulse, only the second pulse is recorded. The important result of the Figure 4 is that that it is possible to separate each pulse individually from a dense-packed package of optical pulses with period of only 450 fs. Only a selected pulse solely creates the spin polarization. Either the following or preceding unselected pulse does not affect the spin polarization. When the clock is at the position of the first pulse (0 ps), the second pulse does not excite any spin-polarization. Therefore, it does not affect the recording. When the clock pulse is at 450 fs, only the second pulse is recorded, but the first pulse does not influence the recording.

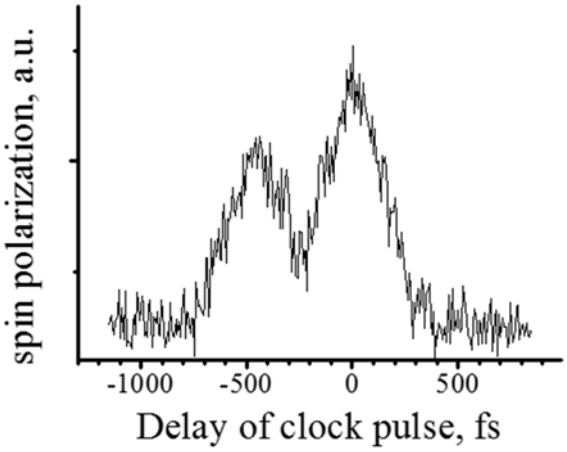

Figure 4. Spin-polarization of electrons excited by the combined beam of clock pulse and two data pulses as a function of the delay of the clock pulse. Reading of the spin-polarization was done 100 ps after arrival of pump pulses. The data proves a feasibility for recording at 2.2 TBit/s. Reproduced with permission from [12], American Institute of Physics, 2009.

For example, in the case when the delay line of 450 fs use in the scheme of Figure 3, the first and second pulses of the date package are stored in each memory element separately. The magnetization of the nanomagnet of the first memory cell is reversed according to whether the first pulse exists or not. The existence or absence of the second pulse does not influence the nanomagnet of the first memory. Similarly, the magnetization reversal of nanomagnet of the second memory cell is triggered only by the second pulse. The existence or absence of the first pulse has no effect on the nanomagnet of the second memory cell.

It should be noted that the reason for the described high-speed demultiplexing is not the ability of high-speed switching of the circular polarization, but a very short relaxation time of the proposed demultiplexing mechanism. The relaxation time of the described spin switching mechanism is the electron dephasing time, which is very short. The following explains why the electron dephasing time is the relaxation time of the described demultiplexing mechanism. When two linear cross-polarized pulses overlap, their combined polarization is circularly-polarized and they excite the spin-polarized electrons. When the pulses are separated, so they are not overlapped, there is no circular polarization

and the spin-polarized electrons should not be excited. This is not correct. For example, in the experiment shown in Figure 4 the autocorrelation measurements showed that, at the delay of 225 fs between a 100-fs wide clock pulse and the pulses of the data package, there is no any overlap between any two pulses. This means that for this delay, the three linear-polarized pulses without any circular polarization component excite the photo electrons. Even though there is no circular polarization of light, still, a substantial spin polarization of the photo-electrons is created (see Figure 4). This can be explained as follows: Within the electron dephasing time the photo-excited electrons are coherent, they conserve their phase and spin. When electrons are excited by two pulses with an interval shorter than the electron dephasing time, the photo-excited electrons interact coherently and they may create a spin- polarization [12]. Therefore, after the illumination by the first linear-polarized-pulse, the material keeps information about the phase of this pulse for a very tiny moment of 450 fs. If within this time, the second pulse illuminates the material, the spin polarization is created, because the information about the phase of the first pulse is still stored in the material. In the case where the second time arrived after a time longer than the electron dephasing time, the information of the phase of the first pulse is lost and the spin polarization cannot be created. This explains the ultra-fast switching speed of the proposed demultiplexing mechanism.

3. High-Speed Injected of Photo-Excited Electrons into a Nanomagnet

The recoding mechanism of the proposed memory consists of two steps (See Figure 1). As was shown above, we have successfully verified an ultra-high demultiplexing for the proposed recording method. The second step of the recording is magnetization reversal of a nanomagnet by spin-polarized photo-excited electrons. This step can be done at a moderate speed.

The spin lifetime in the semiconductor is short. For GaAs it does not exceed 100 picoseconds at room temperature. In the design of the proposed memory a short optical pulse excites spin-polarized electrons in the semiconductor photo-detector. Under the applied voltage the photo-excited electrons are injected into the nanomagnet. In the case when the injection time is longer than the spin lifetime, the spin information is lost inside the semiconductor before it is injected into the nanomagnet.

Additionally, for the same energy of the optical pulse, the amplitude of the injected current lowers for the longer injection time. Since the magnetization reversal has a threshold with respect to the amplitude of the injected current, the long injection time significantly limits the possibility of the magnetization reversal by the light. The injection time shorter than 100 picoseconds is essential to achieve magnetization reversal by the light with respect to both the electron spin lifetime and the amplitude of the injected current. The injection time should be as short as possible. At least it should be shorter than the spin lifetime in the semiconductor.

In order to verify and to optimize the injection of photo-electrons into a nanomagnet, we have fabricated a simplified memory cell comparing to that of Figure 2. We have removed the waveguide and we have made a p-contact directly to the p-region of the photo-detector. Except for this simplification, the structure remains the same as in Figure 2. A femtosecond pulse laser was used as the light source with pulse width of 140 fs and the pulse repetition rate of 80 MHz. The laser beam was focused into a spot of 4-μm diameter exactly on top of nano contact (Figure 5b). Since the size of the nanomagnet and its connecting electrode are much smaller that the laser spot, almost all of the light is absorbed by the photo-detector. The time response of the p-i-n photo detectors was measured by a sampling oscilloscope on a 50-Ohm load resistor connected between the nanomagnet and the metallic contact to p-GaAs layer of the detector. We have found that the injection time strongly depends on the contact resistance between the nanomagnet and the detector. The lowest contact resistance is required to achieve the acceptably-short injection time. In order to reduce the contact resistance we have used a delta-doped InGaAs contacting layer. The same fabrication method was used as was described in the previous chapter. By varying the doping concentration of the InGaAs layer, three samples with the contact resistance of 7000, 250, and 30 Ohm/μm^2 were fabricated. All contacts were Ohmic. Figure 5b shows the time evolution of photo-excited current. For the sample with the contact

resistance of 30 Ohm/μm^2, the injection time was 80 ps, which is shorter than the spin lifetime in GaAs. From Figure 5b it could be concluded the lowest metal/semiconductor contact resistance is a critical parameter for the design of this memory. It should be lower than 100 Ohm/μm^2.

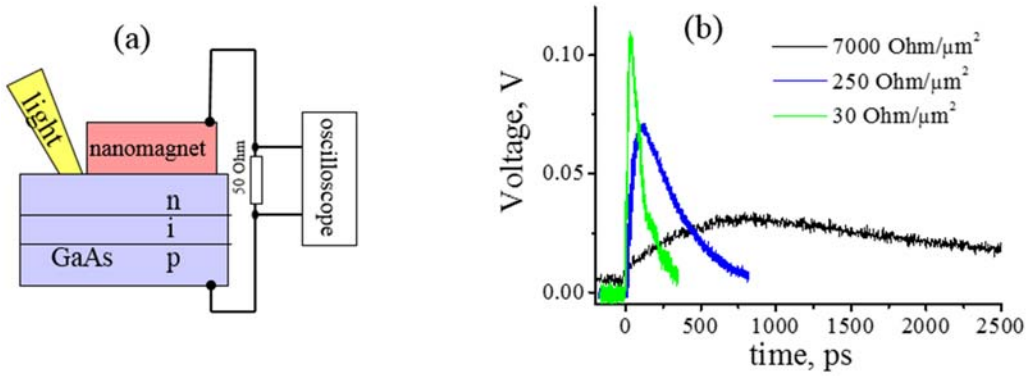

Figure 5. (**a**) Experimental setup to measure the injection time of photo-excited electrons from the p-i-n GaAs photo detector into the Fe nanomagnet; and (**b**) the time evolution of photo-current following excitation by a 140-femtosecond pulse for samples with different nano contact resistance.

There is another reason, which may limit a shortest injection time. The size of the photo detector should be longer than the penetration length of light into the GaAs, which is about 1–2 μm. Therefore, the length of the photo detector should be at least 3–4 μm (See Figure 2). A photo-electron, which is excited at the edge of the photo detector, should pass a distance about 1–2 μm until it reaches the nanomagnet. It takes a time, which may elongate the injection time. In order to verify this we performed the experiment shown in Figure 6. The time evolution of photo-excited current was measured for two cases. At first, the light beam was focused exactly at the center of a nanomagnet and the injection time was measured. Next, the beam was moved 6 μm out of the nanomagnet and the injection time was measured again. As can be seen from Figure 6b, there is a delay of 80 ps between time responses. This means that the photo-excited electrons moves at a speed of 75 km/s = 6 μm/80 ps, which is close to the saturation speed in GaAs. The saturation speed is the fastest speed at which an electron may move in a solid. At a faster speed an electron emits phonons intensively, which rapidly slows it down. The case is similar to the case of a plane flying at an ultrasonic speed.

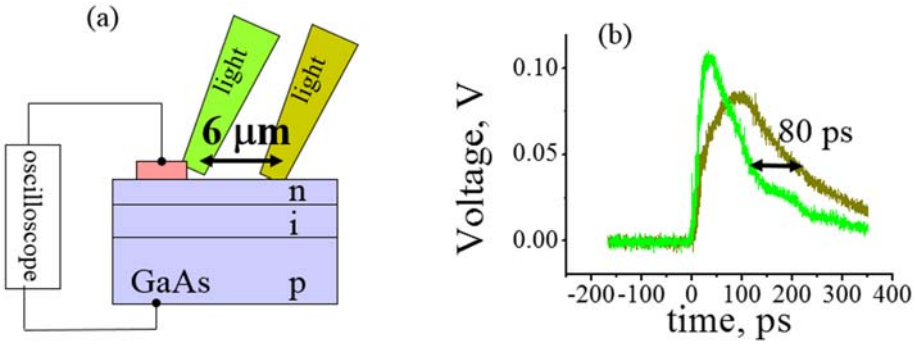

Figure 6. (**a**) Experimental setup to measure the movement speed of photo-excite electrons under injection into the nanomagnet; and (**b**) the time evolution of photo-current in cases when beam is focused at the center of a nanomagnet (light-green line) and 6 mm aside (dark-green line).

For the design in Figure 2, an electron, which is photo-excited at the edge of the detector, needs to move 2 μm until it reaches the nanomagnet. In the case of a sufficiently low contact resistance

of the nanomagnet, it takes only 26 ps. This is a sufficiently short time to ensure that the injected photo-excited electrons are still spin-polarized.

4. Read-Out Mechanism

The magneto-optical effect may be used as a high-speed reading mechanism. The magneto-optical read-out can be achieved by utilizing an effect of magnetization-dependent loss. When one layer of the optical waveguide is a ferromagnetic metal and its magnetization is perpendicular to the mode propagation direction, the optical absorption is different for two opposite direction of the magnetization [13–16]. Therefore, such a waveguide can function as an optical gate, when the light can be switched on or off by reversing the magnetization of the metal. The magnetization of a ferromagnetic metal can be detected by the intensity of transmitted light. Figure 7 shows the transmission light in a transparent AlGaAs waveguide with an embedded Fe nanomagnet as a function a magnetic field applied perpendicularly to the waveguide. In the case of a long nanomagnet, the on/off ratio is high and the signal-to-noise ratio (SNR) is low. As the size of the nanomagnet decreases, the on/off ratio decreases and the SNR increases. It is difficult to read the magnetization of a nanomagnet 1 μm in size or smaller [17]. It should be noted that there is only one mode in the waveguide and there are no other modes to which light could be diffracted. Therefore, there is no any diffraction and there is not any diffraction limit. Still, it is unclear why the on/off ratio sharply decreases and the SNR sharply increases when the size of nanomagnet approaches the light wavelength. The probable reason might be that a surface plasmon is excited on the surface of the ferromagnetic metal [18,19].

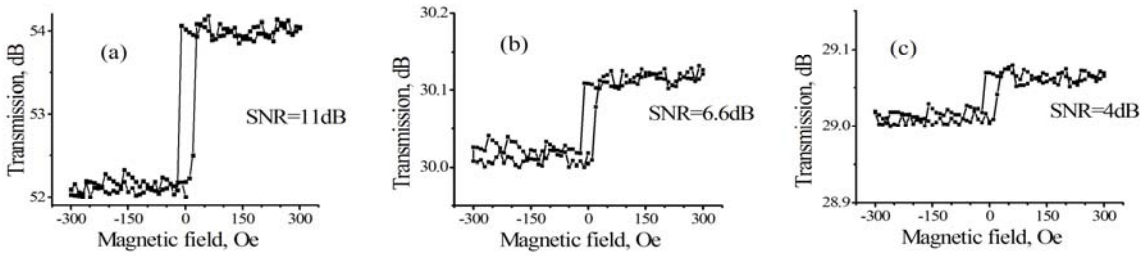

Figure 7. Transmission of transverse-magnetic (TM) mode of rib waveguide with an embedded Fe micromagnet as a function of magnetic field applied perpendicularly to the waveguide and in waveguide plane. Length of nanomagnet is (**a**) 64 μm, (**b**) 8 μm, and (**c**) 4 μm.

5. Memory with a MTJ Electrode

In previous chapters a design of the high-speed memory, which is made of a single ferromagnetic metal (for example, an iron-made nanomagnet) was discussed. There is another possible design of the memory, where a magnetic tunnel junction (MTJ) is used instead of the nanomagnet. There are merits and demerits of such design. Major merit of the memory with a MTJ electrode is its ability for both electrical and optical reading and writing. Due to this property, the reading/recording from/into the memory can be done either by an electrical current, which makes possible a data exchange between the memory and other electrical components inside the chip, or by light, which provides data exchange with other chips. Therefore, this memory design is quite suitable for chip-to-chip connection as a high-speed buffer memory.

The demerit of this design is that the recording can be done not only by a circularly-polarized optical pulse, but also by a linear-polarized pulse. It makes it more difficult to use the high-speed demultiplexing scheme of Figure 3. In contrast to the memory with a nanomagnet, in the case of the memory with a MTJ electrode there are additional limitations on pulse intensities and the number of pulses in a pulse package that could be recorded.

The magnetization direction of a ferromagnetic metal may be reversed by a spin current. The relaxation of spin current in the ferromagnetic metal induces a spin torque [20], which may reverse

the magnetization of the metal. This effect is used as a writing method in magnetic random access memories (MRAM) [5]. In the memory design with a MTJ electrode, the spin current may be generated not only in the semiconductor detector, but also at the tunnel junction. Only circularly-polarized light photo-excites a spin-polarized current in the detector. In contrast, a pulse of any polarization may induce a spin-current and the spin torque at the tunnel barrier. The tunnel barrier itself functions as a spin polarizer. The ability of the magnetization reversal by both spin-polarized and spin-unpolarized photo-currents has some advantages and disadvantages for the memory with a MTJ electrode, which are discussed below.

Figure 8 shows an example of the memory with a MTJ electrode. It consists of a GaAs p-i-n diode with a MTJ electrode and a side electrode in close vicinity of the MTJ electrode. The MTJ is made of two ferromagnetic metals separated by an MgO tunnel barrier. The "free" layer of the MTJ is in contact with the GaAs photodiode. The top layer of the MTJ is the "pin" layer. The photo-induced electrons may reverse magnetization of the "free" layer, but the magnetization of "pin" layers should remain the same. The magnetization direction of "free" and "pin" layers may be either in-plane, as shown in Figure 8, or perpendicular to the plane. The resistivity of the MTJ depends on mutual orientation of magnetization of "free" and "pin" layers. The "free" layer has two opposite stable magnetization directions. The data is stored as a magnetized direction in the "free" layer. The side contact is used for the electrical recording and reading. There is a delta-doped nn-InGaAs layer (which is not shown in Figure 8) between the "free" layer of MTJ and n-GaAs. As was explained before, the nn-InGaAs layer is used to achieve the lowest contact resistance between the MTJ and n-GaAs layer. Additional difference of the design of Figure 8 from the design of Figure 2 is that the p-i-n detector is embedded into the AlGaAs waveguide. The AlGaAs was wet-etched before the growth of the detector.

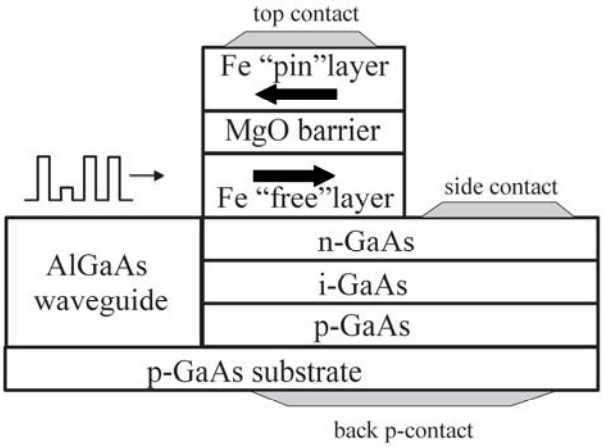

Figure 8. Design of spin-photon memory with magnetic tunnel junction (MTJ) electrode.

In the memory with a MTJ electrode recording and reading can be done by an electrical current. The recording and reading methods are similar to those that are currently used in the MRAM [5].

For the electrical reading, a voltage is applied between the MTJ and the side contact. The resistivity of the MTJ is different for two opposite magnetization directions of the "free" layer with respect to the magnetization direction of the "pin" layer. The stored data is sensed by the current flowing through the MTJ.

For the electrical recording, a larger voltage is applied between the MTJ and the side contact. The charge current, which flows through the tunnel barrier, induces the spin current. The relaxation of the spin current causes a spin-transfer torque [20]. The spin-transfer torque is a consequence of the transfer of spin angular momentum from a spin current. If the current is sufficient, the magnetization of the "free" layer is reversed by the spin-transfer torque and data is memorized. By changing polarity

of the applied voltage, the magnetization of the "free" layer can be turned either in parallel or opposite to the magnetization of the "pin" layer.

The method of the optical reading for this memory is based on the control of the optical gain of a p-i-n junction by a MTJ electrode. The p-i-n GaAs junction absorbs the light, when there is no current injection into the p-i-n junction. When under a direct bias the current is injected, the absorption can be compensated and light can be amplified, because of the stimulated emission. A bias voltage is applied between the back electrode and the top of the MTJ. Since the different resistance of the MTJ, the current injected into the p-i-n GaAs is different for the opposite magnetization directions of the "pin" layer. The bias voltage should be optimized so that for the parallel magnetization directions of the MTJ electrodes, the injection current is sufficient to produce an optical gain in the p-i-n junction and, for the opposite magnetization directions, the injection current should not be sufficient to create any gain. Therefore, the direct-biased p-i-n junction with a MTJ works as an optical switch. When the magnetization of the "free" layer is parallel to the magnetization of the "pin" layer, a light pulse can pass through the junction. When the magnetization of the "free" layer is reversed, the light pulse is blocked.

Figure 9 shows IV characteristic of a p-i-n junction with a MTJ electrode, in which the magnetization of the "free" layer is either parallel or opposite to the magnetization of the "pin" layer. The data was calculated from the measured IV characteristics of a fabricated nano-sized MTJ contact and micro-sized p-i-n GaAs junction. The operation voltage was optimized that the amplifier provides a gain when the magnetizations of the "pin" and "free" layers are in parallel. The amplifier absorbs the light when the magnetization directions are opposite. Therefore, the optical amplifier is either transparent or not depending on the magnetization direction of the "free" layer or the data stored in the memory cell.

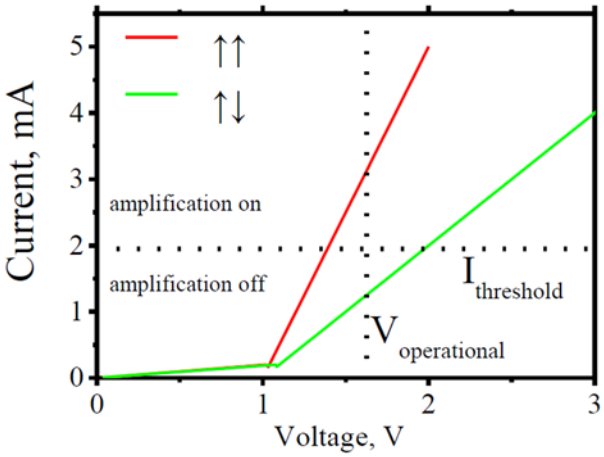

Figure 9. IV characteristic of p-i-n optical amplifier with MTJ electrode. The arrows show mutual magnetization directions of the "free" and "pin" layers. The red line shows the case when the magnetization of the "free" layer is parallel to the magnetization of "pin" layer. The green line shows the case when the magnetization of the "free" layer is opposite to the magnetization of the "pin" layer. The data were calculated from the measured IV characteristics of fabricated a nano-sized MTJ and a micro-sized GaAs p-i-n junction. Above the threshold current the amplifier provides a gain. The optimum operation voltage is shown. At the optimum voltage the optical amplifier is either transparent for light or not transparent depending on the data stored in the memory cell.

High-speed read-out of the optical memory is called multiplexing. The output of the multiplexing is a package of optical pulses. The intensity of each pulse is proportional to the data stored in a corresponded memory element. The pulse width and the interval between pulses should be as short as possible. Figure 10 shows the multiplexing scheme. The mode-locked laser provides a short pulse.

The waveguide path is split so that the pulse is split and it illuminates every memory cell. A pulse can pass a memory cell for one magnetization direction and is blocked for the opposite magnetization direction. At the output, all waveguide paths are combined. Each path has different length, so that each pulse reaches the output with a different delay and the amplitude of the pulse corresponded to the "free"-layer magnetization of each cell. Therefore, at the output the serial train of pulses is created. The intensity of each pulse is proportional to the data stored in each memory cell. The speed of the reading is limited only by a shortest pulse width, for which the p-i-n junction is still able to provide an optical gain.

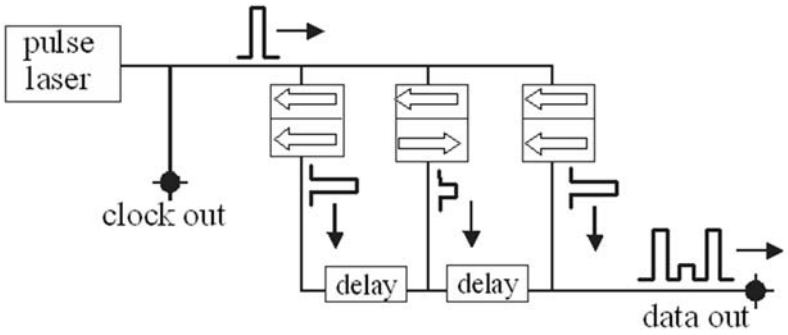

Figure 10. Multiplexing scheme for high-speed reading of the memory with MTJ electrode.

As was explained above (See Figure 7), the high-speed reading of magnetization of a nanomagnet was demonstrated for nanomagnet length of 1 μm or longer [17]. There are difficulties for the magnetization reading for nanomagnets of a smaller size. For the magnetization reading of a nanomagnet length of 1 μm or shorter, both the on/off ratio and the SNR sharply decrease [17]. In contrast, in the case of the magnetization reading of memory with a MTJ electrode, both the on/off ratio and the SNR do not depend on electrode size. Therefore, the high-speed optical reading is still possible even for nanomagnet diameters of 100 nm or smaller.

The method of high-speed optical recording for the memory with MTJ is similar to that of the memory with a nanomagnet. The circularly-polarized optical pulse is absorbed in the p-i-n GaAs junction creating spin-polarized electrons. Under the bias voltage applied between MTJ and back electrode these spin-polarized electrons are injected from the semiconductor into the "free" layer of MTJ. The spin transfer torque is a consequence of the transfer of spin angular momentum from a spin-polarized current to the magnetic moment of the "free" layer of the MTJ. If the torque is sufficient, the magnetization turns and the data is recorded.

There are both merits and demerits for the recording when a MTJ electrode used instead of a nanomagnet. The main advantage is that the recording can be done by an optical pulse of a substantially-smaller intensity. It can be realized as follows: in addition to the bias voltage, which is applied between the back electrode and the top of the MTJ, a voltage can be applied between the side contact and the MTJ. The current, which flows between the side and MTJ electrodes, should be adjusted just slightly below the threshold current for the magnetization reversal of the "free" layer of the MTJ. In this case an optical pulse of a small intensity can trigger the magnetization reversal. Therefore, a pulse of a smaller intensity can be memorized.

In contrast to spin-photon memory with a nanomagnet, in the case of the memory with MTJ, a linear-polarized pulse of sufficient intensity may reverse the magnetization of the "free" layer. This is an undesirable event. In the scheme of the high-speed demultiplexing (Figure 3), the recorded pulse should be circularly polarized. Other pulses in the optical package are linearly polarized and should not have any influence on the recording. It is not the case of the memory with a MTJ electrode. The linearly-polarized pulses may have a substantial influence on the recording. Still, it is possible to use the demultiplexing scheme of Figure 3 for the memory with a MTJ electrode.

The memory should be optimized to make the threshold current for the magnetization reversal by a spin-polarized current to be significantly smaller than the threshold current for the reversal by a spin-non-polarized current. This can be done by decreasing the spin polarization of a material of the "pin" layer.

The fabrication of the MTJ on top of a semiconductor photo detector with very thin tunnel barrier and very thin free layer on top of the semiconductor is the main challenge of the fabrication of the memory with a MTJ electrode. The following explains the importance of a thin tunnel barrier, a thin free layer, and a low semiconductor/metal contact resistance for the fabrication of the memory with a MTJ electrode.

From MRAM technology [5] it is known that there is a threshold current, above which the current-induced magnetization reversal is possible. Typically, the threshold current density is about 1×10^7 A·cm^2. The requirement of a high current density limits the variation of parameters of the MTJ. The first limitation is on the size and thickness of the "free" layer. Since the threshold current is proportional to the volume of the "free" layer. The thickness of the "free" layer should be thinner than 2 nm and its diameter should be smaller than 100 nm. The second limitation is with respect to the thickness of the MgO tunnel barrier. The maximum voltage, which may be applied to a MTJ is about 1 V. A higher voltage breaks the tunnel barrier. In order to achieve the required high current at this upper-limit voltage, the MTJ resistance should be sufficiently low. It limits the thickness of the MgO tunnel barrier to be smaller than 1.3 nm. The third limitation is with respect to the contact resistance between the MTJ electrode and the semiconductor. Since the contact resistance and the MTJ resistance are in series, the contact resistance should be comparable or smaller than the MTJ resistance. This limits the contact resistance to be smaller than 50 Ohm/μm^2. As was explained above (see Figure 5b), we were able to fabricate the samples with a contact resistance of 30 Ohm/μm^2, which fits this requirement well.

We have succeeded in fabricating a nano-sized MTJ contact on a GaAs photo-detector, in which tunnel magneto resistance (TMR) is about 100%. However, we were able to fabricate the MTJ with the high TMR only in the case when the "free" layer is thicker than 12 nm and the MgO barrier is thicker than 1.7 nm. As was mentioned above, both thicknesses should be reduced to meet the requirements for the magnetization reversal. It is possible to decrease the thickness of the MgO barrier down to 1.3 nm, but this causes the decrease of the TMR to 40%–70% and the decrease of the number of good samples on wafers without pin holes. The yield reduces from 99% to 10%. It is more difficult to reduce the thickness of the "free" layer. Even a slight decrease in the thickness of the "free" layer causes a sharp drop of the TMR. We have found the reason for the drop of the MR is the diffusion of Ga, As, and In into the region in the vicinity of the tunnel junction. In order to reduce the diffusion we have used the following growth procedure: after a semiconductor growth, a sample was cooled to -10 °C and the Fe "free" layer and 0.7-nm of the MgO barrier were grown. Then, the sample was heated up to 200 °C and the remaining part of the MgO barrier was grown. The "pin" layer was grown at room temperature. The low-temperature growth suppresses the diffusion and a higher-temperature growth of the MgO is required to make a smoother tunnel barrier. Figure 11 shows the measured TMR as a function of thickness of the "free" layer for different thicknesses of the MgO barrier. Even in the case of the optimized growth, the TMR drops below 10 nm and it nearly vanishes at a "free" layer thickness of 5 nm. The distributions of Ga, In, and As across the thickness of the "free" layer was measured by the secondary ion mass spectrometry (SIMS). The Ga, In, and As were detected within thickness of the "free" layer of 5 nm.

Even though the amount of the Ga, In, and As in the vicinity of the tunnel is very small and it does not exceed 0.1%, the contamination causes a substantial drop of the TMR. The reason for this undesirable effect still has to be understood.

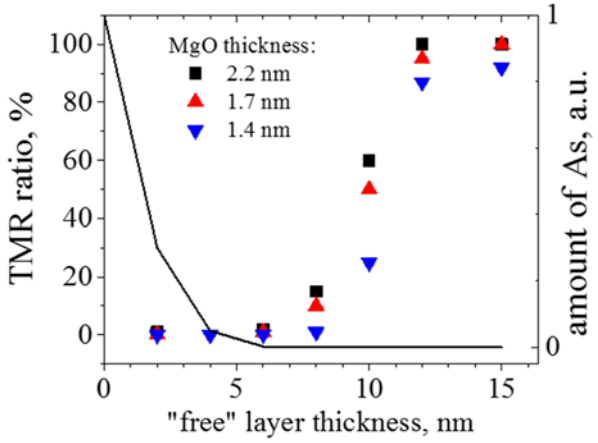

Figure 11. Tunnel magneto-resistance of Fe/MgO/Fe MTJ grown on a p-i-n GaAs photodetector as a function of thickness of "free" layer. The dark line shows the distribution of As contamination across the thickness of the "free" layer.

In order to verify the possibility of the magnetization reversal by photo-excited electrons we have studied the sample shown in Figure 12a. The thickness of the "free" layer was 8 nm. The TMR is still substantial at this thickness. Even though the "free" layer was too thick to expect the magnetization reversal, a spin precession, which is induced by the photo-excited electrons, could be expected. A light beam was focused into a 4-μm-diameter spot with the MTJ contact at the center. A femtosecond pulse laser was used as the light source with the pulse width of 140 fs and the pulse repetition rate of 80 MHz. A femtosecond light pulse generates photo-carriers in the p-i-n GaAs, which is injected into the lower electrode of the MTJ. The TMR was measured under illumination of light as follows. A voltage drop at the MTJ was measured using the side electrode by a DC voltmeter. The photocurrent was measured by a DC ammeter connected between the top of the MTJ and the p-GaAs contact. From these data the resistance of the MTJ was calculated.

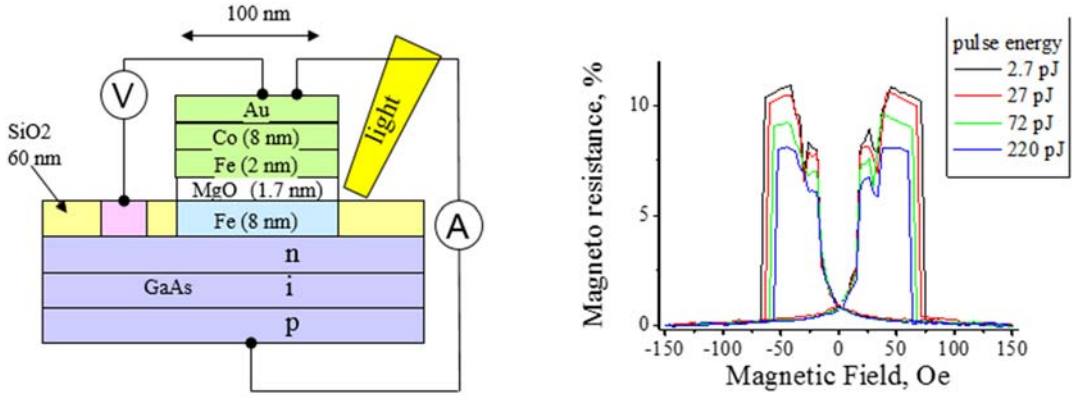

(**a**) (**b**)

Figure 12. (**a**) Experimental setup for the measurement of the TMR of the Fe/MgO/Fe MTJ fabricated on top of the p-i-n-GaAs photo detector under illumination of femtosecond pulses. The diameter of the MTJ electrode is 100 nm; and (**b**) magneto resistance of the MTJ electrode measured under illumination of femtosecond pulses of different energy.

Figure 12b shows the magneto-resistance of the Fe:MgO:Fe MTJ measured under illumination of femtosecond pulses of different energies. The TMR decreases as the pulse energy increases. In addition, the switching field of the top Fe/Co "pin" electrode (the switching field is ~60 Oe)

decreases as the pulse energy increases. In contrast, the switching field of the lower Fe "free" electrode (the switching field is a ~15 Oe) does not depend on the pulse energy. We did not observe a difference in the TMR measured for linearly and circularly polarized light.

There may be several reasons for the observed dependence of the TMR on the pulse energy. The first reason might be the thermo heating. However, the average pulse energy was too small to cause a substantial heating. The average pulse energy was only 0.216 mW, 2.16 mW, 5.76 mW, and 17.6 mW, respectively. Our simulation by the finite-difference method estimates that the temperature increase should not exceed a few degrees. The second reason might be the voltage-dependence of the TMR. The voltage measured by the DC voltmeter was 6 mV, 38 mV, 65 mV, 153 mV, respectively. Even though the real AC voltage is larger (See Figure 5b), still the voltage is too small to cause the reduction of the TMR. The third reason might be the magnetization precession of the electrodes of the MTJ induced by the spin transfer torque. The current measured by the DC ammeter was 8, 52, 89 and 210 μA, respectively. The corresponded DC current density is calculated as 7×10^3, 4.4×10^4, 7.6×10^4 and 1.8×10^5 A/cm^2. The DC current density is too small to start the magnetization precession. However, as can be seen from Figure 5b, there is a large spark of photo-current during the first ten picoseconds after the arrival of the optical pulse. This spark of photo-current may initialize the spin precession.

6. Conclusions and Perspectives

We have proposed, fabricated, and studied a high-speed non-volatile optical memory. We have demonstrated experimentally that it is possible to switch spin polarization at a very high speed. It was shown that one selected pulse from a package of two optical data pulses with the interval of 450 fs can solely excite the spin-polarized electrons without a disturbance from the unselected optical data pulse. Since the memory is designed so that only spin-polarized electrons can be recorded, it proves the feasibility of the proposed memory to record data with the rate of 2.2 Tbits/s. The fast recording speed of this memory benefits from the short electron dephasing time in semiconductors.

We have shown that an ultra-low contact resistance between a semiconductor and a nanomagnet is the critical parameter, which is required in order to achieve a high-speed injection of photo-excited electrons from a semiconductor and a nanomagnet within a time shorter than a spin lifetime. We have achieved a contact resistance as low as 30 Ohm/μm^2 between a Fe nanomagnet and n-GaAs. We have demonstrated the injection of the photo-excited electrons into the nanomagnet within the time interval of 80 ps, which is shorter than the spin life time in the GaAs.

The high-speed reading can be done using the magneto-optical (MO) effect of the magnetization-dependent loss. We have demonstrated experimentally the read-out of nanomagnets of sizes larger than 1 μm with a high SNR and a high on/off ratio. However, in the case of nanomagnet diameter of 1 μm or smaller, the on/off ratio and the SNR sharply decrease. This makes difficult to use this MO read-out method for nanomagnets of a smaller size.

The problem can be resolved using a spin-injection from a nanomagnet into a gain region of an optical amplifier [17]. The spin-polarized electrons, which are injected from a nanomagnet into the amplifier, spread over a larger volume in the amplifier. This makes the effective volume of a MO material larger and the read-out easier. The read-out efficiency may be improved even more in a memory with a MTJ electrode. The resistance of the MTJ significantly changes for two opposite directions of the "free" layer due to the TMR effect. In the case when the MTJ is used as an electrode of an optical amplifier, the reversal of the magnetization may switch on/off the optical amplifier. This reading method is very effective. It provides a large SNR and a high on/off ratio for reading.

The magnetization reversal by the photo-excited electrons is the main challenge to realize high-speed recording, which yet has to be demonstrated. At present, the major obstacle for this is the degradation of magnetic properties of a nanomagnet in regions in close vicinity of the semiconductor interface. It causes a sharp decrease and vanishing of the TMR effect. At present, only the use of a thicker "free" layer, which separates the MTJ from the semiconductor interface, restores a high TMR.

However, in the case a thicker "free" layer the magnetization reversal by photo-current is impossible, because it requires an unrealistically large photo current. A possible solution of this problem is the usage of a diffusion block layer at the semiconductor interface. It is critically important that the diffusion-blocking layer should not comprise the low contact resistance between a nanomagnet and a semiconductor. Finding a suitable material for the diffusion-blocking layer is a challenging task.

For the successful operation of the proposed memory all steps for recording and reading should be demonstrated and optimized in a single device. At present, only a part of these steps has been successfully demonstrated. Some efforts are still required to demonstrate the "full" operation of the memory. However, when all the present issues will be resolved, the compact, integratable, non-volatile, and ultra-high-speed optical memory may have a significant impact on many different applications.

Acknowledgments: This work was financially supported by New Energy and Industrial Development Organization (NEDO) and by Japan Society for the Promotion in Science (Kakenhi).

Conflicts of Interest: The authors declare no conflict of interest.

References

1. Gnauck, A.H.; Charlet, G.; Tran, P.; Winzer, P.J.; Doerr, C.R.; Centanni, J.C.; Burrows, E.C.; Kawanishi, T.; Sakamoto, T.; Higuma, K. Terabit Transmission at 42.7-Gb/s on 50-GHz Grid Using Hybrid RZ-DQPSK and NRZ-DBPSK Formats Over 16 × 80 km SSMF Spans and 4 Bandwidth-Managed ROADMs. *J. Lightwave Technol.* **2008**, *26*, 79–84. [CrossRef]
2. Sun, C.; Wade, M.T.; Lee, Y.; Orcutt, J.S.; Alloatti, L.; Georgas, M.S.; Waterman, A.S.; Shainline, J.M.; Avizienis, R.R.; Lin, S.; et al. Single-chip microprocessor that communicates directly using light. *Nature* **2015**, *528*, 534–538. [CrossRef] [PubMed]
3. Arakawa, Y.; Nakamura, T.; Urino, Y.; Fujita, T.; Mogami, T.; Horikawa, T.; Kinoshita, K.; Sasaki, H.; Morito, K.; Kurata, K. Silicon photonics for next generation system integration platform. *IEEE Commun. Mag.* **2013**, *13*, 72–77. [CrossRef]
4. Chang, Y.-F.; Fowler, B.; Zhou, F.; Lee, J.C. Intrinsic Unipolar SiO_x-based Resistive Switching Memory: Characterization: Mechanism and Applications. *ECS Trans.* **2015**, *69*, 149–164. [CrossRef]
5. Ando, K.; Fujita, S.; Ito, J.; Yuasa, S.; Suzuki, Y.; Nakatani, Y.; Miyazaki, T.; Yoda, H. Spin-transfer torque magnetoresistive random-access memory technologies for normally off computing. *J. Appl. Phys.* **2014**, *115*, 172607. [CrossRef]
6. Blumenthal, D.J.; Barton, J.; Beheshti, N.; Bowers, J.E.; Burmeister, E.; Coldren, L.A.; Dummer, M.; Epps, G.; Fang, A.; Ganjali, Y.; et al. Integrated Photonics for Low-Power Packet Networking. *IEEE J. Sel. Top. Quantum Electron.* **2011**, *17*, 458–471. [CrossRef]
7. Burmeister, E.F.; Blumenthal, D.J.; Bowers, J.E. A comparison of optical buffering technologies. *Opt. Switch. Netw.* **2008**, *5*, 10–18. [CrossRef]
8. Heck, M.J.R.; Kurczveil, G.; Burmeister, E.F.; Park, H.; Mack, J.P.; Blumenthal, D.J.; Bowers, J.E. Integrated Recirculating Optical Buffers. *Proc. SPIE* **2010**, *7606*, 76060W.
9. Takahashi, R.; Nakahara, T.; Takahata, K.; Takenouchi, H.; Yasui, T.; Kondo, N.; Suzuki, H. Photonic random access memory for 40-Gb/s 16-b burst optical packets. *IEEE Photonics Technol. Lett.* **2004**, *16*, 1185–1187. [CrossRef]
10. Nozaki, K.; Shinya1, A.; Matsuo, S.; Suzaki, Y.; Segawa, T.; Sato, T.; Kawaguchi, Y.; Takahashi, R.; Notomi, M. Ultralow-power all-optical RAM based on nanocavities. *Nat. Photonics* **2012**, *6*, 248–252. [CrossRef]
11. Takahashi, R.; Suzuki, H. 1-Tb/s 16-b All-Optical Serial-to-Parallel Conversion Using a Surface-Reflection Optical Switch. *IEEE Photonics Technol. Lett.* **2003**, *15*, 287–289. [CrossRef]
12. Zayets, V.; Ando, K. High-speed switching of spin polarization for proposed spin-photon memory. *Appl. Phys. Lett.* **2009**, *94*, 121104. [CrossRef]
13. Zaets, W.; Ando, K. Optical waveguide isolator based on non-reciprocal loss/gain of amplifier covered by ferromagnetic layer. *IEEE Photonics Technol. Lett.* **1999**, *11*, 1012–1014. [CrossRef]
14. Zayets, V.; Saito, H.; Yuasa, S.; Ando, K. Enhancement of the transverse non-reciprocal magneto-optical effect. *J. Appl. Phys.* **2012**, *111*, 023103. [CrossRef]

15. Parys, W.V.; Moeyersoon, B.; Thourhout, D.V.; Baets, R.; Vanwolleghem, M.; Dagens, B.; Decobert, J.; Gouezigou, O.L.; Make, D.; Vanheertum, R.; et al. Transverse magnetic mode nonreciprocal propagation in an amplifying AlGaInAs/InP optical waveguide isolator. *Appl. Phys. Lett.* **2006**, *88*, 071115. [CrossRef]
16. Shimizu, H.; Nakano, Y. First Demonstration of TE Mode Nonreciprocal Propagation in an InGaAsP/InP Active Waveguide for an Integratable Optical Isolator. *Jpn. J. Appl. Phys.* **2004**, *43*, L1561–L1563. [CrossRef]
17. Zayets, V.; Saito, H.; Yuasa, S.; Ando, K. Magnetization-dependent loss in an (Al,Ga)As Optical Waveguide with an Embedded Fe micromagnet. *Opt. Lett.* **2010**, *35*, 931–933. [CrossRef] [PubMed]
18. Zayets, V.; Saito, H.; Yuasa, S.; Ando, K. Optical Isolator Utilizing Surface Plasmons. *Materials* **2012**, *5*, 857–871. [CrossRef]
19. Zayets, V.; Saito, H.; Yuasa, S.; Ando, K. Long-distance propagation of a surface plasmon on the surface of a ferromagnetic metal. *Opt. Express* **2015**, *23*, 12834–12839. [CrossRef] [PubMed]
20. Zayets, V. Spin rotation after a spin-independent scattering. Spin properties of an electron gas in a solid. *J. Magn. Magn. Mater.* **2014**, *356*, 52–67. [CrossRef]

© 2017 by the author; licensee MDPI, Basel, Switzerland. This article is an open access article distributed under the terms and conditions of the Creative Commons Attribution (CC-BY) license (http://creativecommons.org/licenses/by/4.0/).